Crack path and fracture surface analysis in VHCF under biaxial loadings

Luís Reis[1,2], Ricardo Pereira[1], Pedro R. Da Costa[1], Diogo Montalvão[3], Manuel Freitas[2,4]

[1]*Instituto Superior Técnico, Av. Rovisco Pais, Lisboa, 1049-001 Lisboa, Portugal*

[2]*IDMEC, Instituto Superior Técnico, Universidade de Lisboa, Lisboa, Portugal*

[3]*Department of Design and Engineering, Bournemouth University, Talbot Campus, Poole BH12 5BB, UK*

[4]*Atlântica, Escola Universitária, Fábrica da Pólvora de Barcarena, 2730-036 Barcarena, Portugal*

Very High Cycle Fatigue *Ultrasonic testing* *Fatigue crack path*

Abstract: Ultrasonic fatigue machines and related investigations are continuously growing in publisher countries and laboratories. They allow researchers to study fatigue in a time and energy reliable manner, fatigue strength and fracture mechanics between 10E06 to 10E10 cycles, the established Very High Cycle Fatigue (VHCF) regime. Almost all published research to date was conducted under uniaxial tension-compression, pure torsion or bending fatigue ultrasonic testing conditions. The interest in biaxial ultrasonic methods for VHCF has begun to evolve from the increasing available knowledge surrounding uniaxial fatigue in VHCF. Tension-Torsion biaxial ultrasonic fatigue tests were first reached by adapting the tension-compression ultrasonic setup. The present work focuses on the crack path and fracture surface analysis and evaluation of different specimens, that failed under different biaxial loading conditions. Observation and analysis of crack initiation and propagation of tested biaxial tension-torsion and cruciform specimens in ultrasonic frequencies was carried out. All evaluated specimens were specially designed and machined to function under ultrasonic fatigue machines resonance concept. Three different biaxial loading paths were carried out, in-phase tension-torsion and tension-tension, and out-of-phase tension-compression. Crack initiation, crack path and crack surface morphologies were analyzed by microscope and scanning electron microscope. Obtained results were analyzed and discussed; conclusions concerning these types of failures under VHCF regime are drawn.

1 INTRODUCTION

Fatigue research is a topic of great interest and importance for a wide range of industries and applications. As methods have continuously been developed and improved since the first investigations by Wöhler, fatigue research is currently exploring the Very High Cycle Fatigue (VHCF) regime between 10E06 and 10E10 cycles. To reach such an elevated number of cycles, is often very costly both in terms of time and energy. Therefore, the emergence of ultrasonic fatigue testing machines provides a great alternative to the study of the VHCF regime in a time and energy reliable way.

Ultrasonic fatigue machines and respective research studies have gained traction with many publications covering different loading conditions, such as uniaxial tension-compression, pure torsion or bending fatigue [1– 6]. However, most publications have presented uniaxial stress states. As with conventional fatigue, research begun by studying more simple uniaxial stress states, with multiaxial fatigue emerging afterwards, once solid knowledge had been established. The same trend can be observed when looking at ultrasonic fatigue research, with publications dedicated to multiaxial fatigue test methods and specific specimen design [2-3],

[7-8]. In general, ultrasonic fatigue testing machines are composed by a piezoelectric transducer, a booster, a horn and finally the specimen to be tested. The piezoelectric transducer often works within a frequency range between 19.45-20.45 kHz. Both booster and horn provide mechanical amplification. As it is well documented [2-6], ultrasonic fatigue testing machines make use of resonance theory in order to generate stress states on test specimens at high frequencies. All components are excited at a resonant mode which is the result of the resonant modes of each individual component. This, in turn, means that each individual component must be designed with the resonant mode of interest within the work frequency range of the piezoelectric transducer. Previous publications show that specimen, horn or both, can be the key to enable multiaxial studies by redesigning these components [2-3].

In this study, a brief overview over the design of multiaxial specimens for different stress states and stress ratios is described. Experimental tests under biaxial loading conditions, i.e. tension-torsion with cylindrical type specimens and Tension – Tension (T-T) and Compression – Tension (C-T) with cruciform specimens in ultrasonic frequencies were carried out. Then fracture surfaces were observed and evaluated, i.e the fracture surface morphology was characterized at the optical microscope and in detail at scanning electron microscope (SEM). Crack initiation angles were measured, and crack propagation features considered and pointed out. Obtained results were analyzed and discussed; conclusions concerning these types of failures under VHCF regime are drawn.

2 MATERIALS AND METHODS

2.1 Ultrasonic Cruciform Specimens

As previously discussed, ultrasonic fatigue test specimens must be designed with resonant modes of interest in mind. For the particular case of the cruciform specimens, the design was carried out following previous work from Baptista *et al.* [9], and also D. Montalvão and A. Wren [3]. These specimens were the focal point of design in order to achieve the target combination between the aimed stress state and resonant mode. A generic illustration of a cruciform specimen ultrasonic fatigue test assembly is presented in Figure 1.

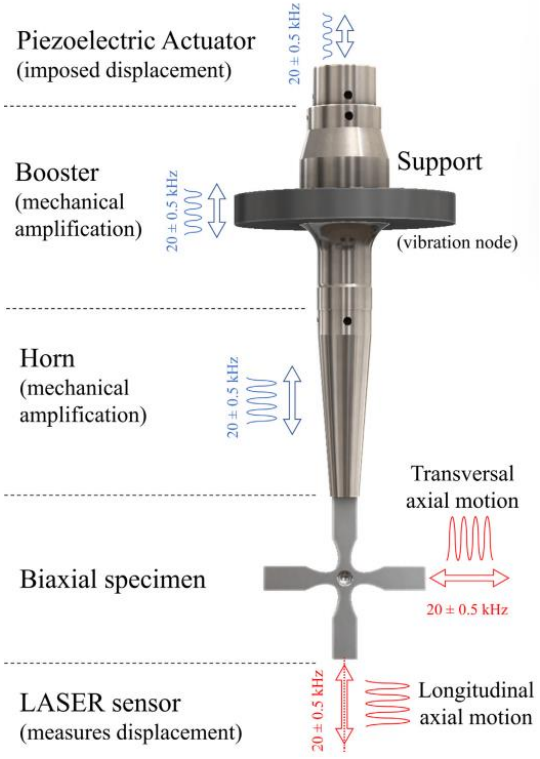

Figure 1 - Generic assembly of an ultrasonic fatigue cruciform test specimen [3].

The cruciform specimens were designed with a clear goal to induce axial-axial stress state with different axial/axial stress ratios. As a result, two slightly different cruciform specimens were designed: one for in-phase Tension-Tension (T-T) (equibiaxial); and another for out-of-phase Compression-Tension (C–T) (pure hear). Figure 2 shows a representation of each type of cruciform specimen.

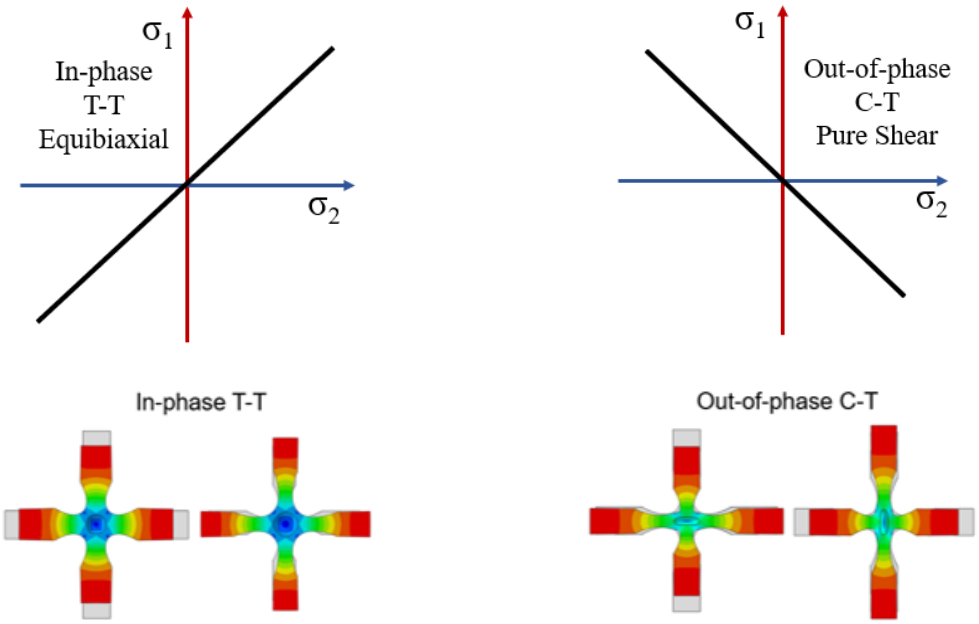

(a) (b)

Figure 2 - Cruciform specimens (a) In-phase Tension-Tension (T-T); (b) Out-of-phase Compression-Tension.

The dimensions of the cruciform specimens were fine tuned resorting to finite element (FE) modal analysis. It was also verified that the desired resonant mode was reached at approximately 20 kHz and the highest stress concentration was achieved in the central region of the specimen. In order to validate the FE results, instrumentation of the central region of the specimens with rosette strain gauges was carried out. Moreover, the specimen displacement at the arm tips was measured using a dual-channel LASER Doppler vibrometer. A schematic representation of the measurement positions and alignment of the rosette strain gauge is provided in Figure 3. All cruciform specimens were manufactured from Aluminium Alloy 6082-T651.

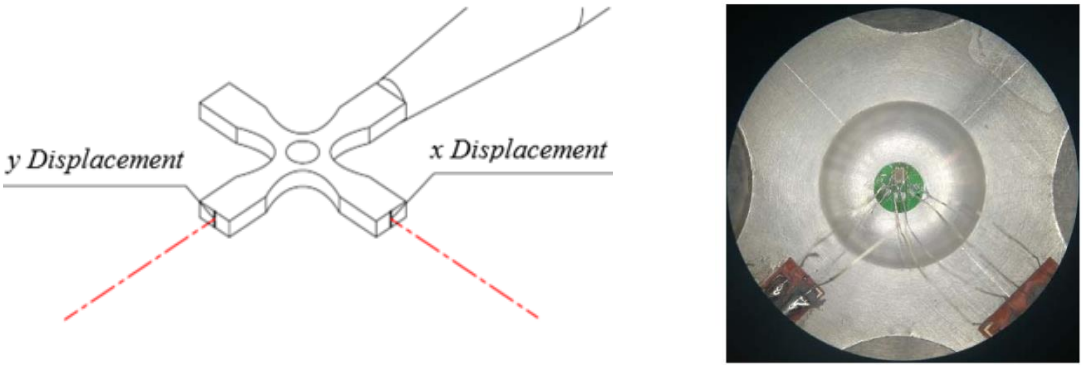

(a) (b)

Figure 3 - Test measurement schematic: (a) Specimen arm tip displacement; (b) Strain Gauge Rosette at central region of specimen.

The cruciform specimens were subjected to ultrasonic fatigue testing until failure. However, complete fracture was not achieved under fatigue testing. This was due to the change in resonant frequency of the specimen provoked by fatigue crack propagation, which leads to a change in specimen stiffness and consequently the resonance effect is lost. The cruciform specimens were fully separated, after the fatigue test, by employing a conventional tensile testing machine.

2.2 Ultrasonic Tension-Torsion Specimens

Similarly, to the cruciform specimens, the tension-torsion specimens required a specific and dedicated design, in order to achieve the desired stress state at an adequate frequency. However, for this particular case the ultrasonic fatigue test contemplates a different design for both specimen and the horn, which provides the mechanical amplification. Following the work presented in [2], the same methodology was followed for the specimen design, considering the previously defined horn. This setup allowed for a tension-compression and torsion stress state to be induced on the specimen in the aimed region. Figure 4 illustrates the assembly of the tension-torsion multiaxial setup.

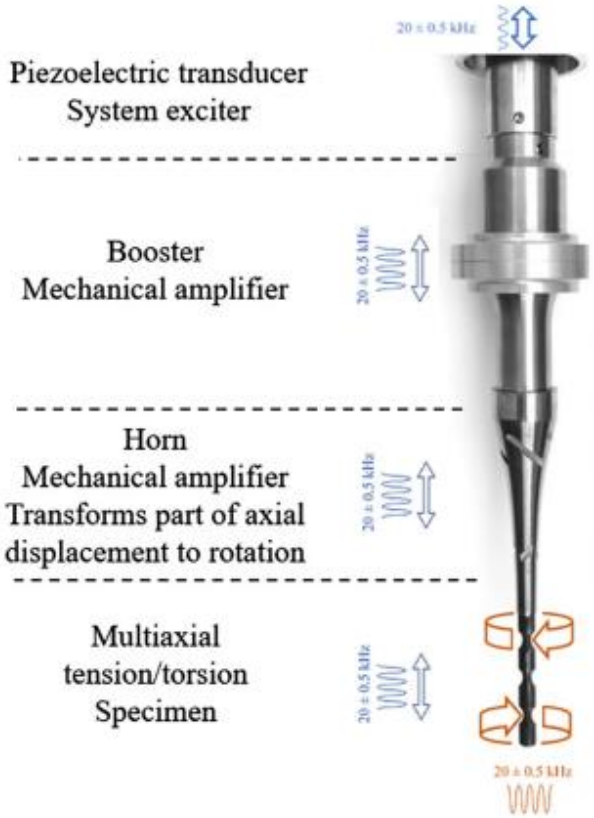

Figure 4 - Tension-Torsion multiaxial setup representation [8].

The geometry of this specimen allows changing the shear/axial stress ratio, by modifying its dimensions [8]. Strain measurements on the tension-torsion specimens were also achieved by using strain gauge rosette. Longitudinal and rotational displacements were measured with a dual-channel LASER Doppler vibrometer, and the schematic representation of displacement and strain measurements is shown in Figure 5. Different shear/axial stress ratio specimens were tested.

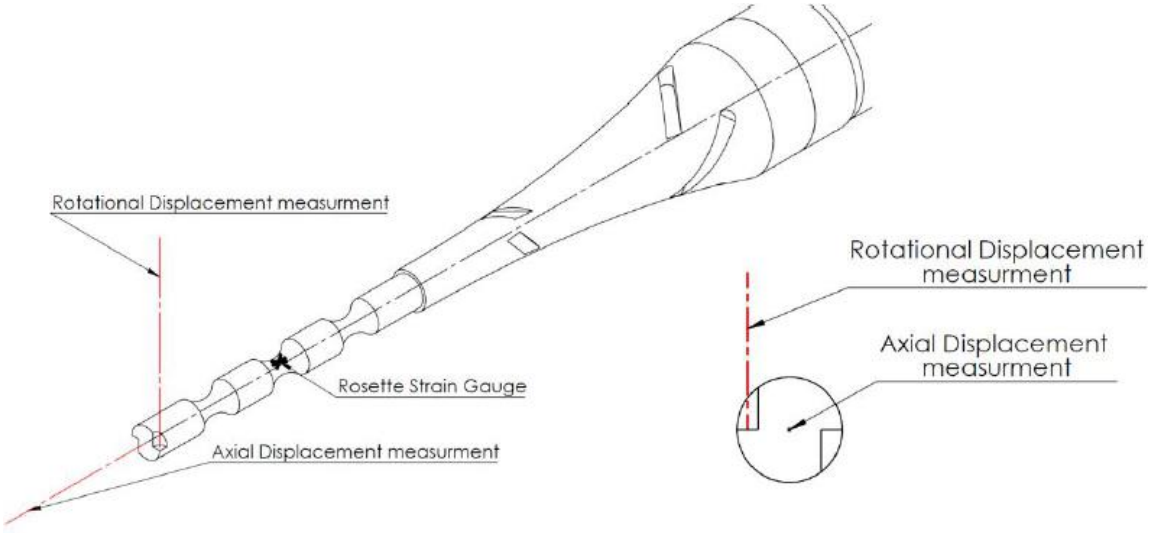

Figure 5 - Tension-torsion displacement and strain measurement schematic.

The tension-torsion specimens were manufactured from AISI P20 steel and were subjected to ultrasonic fatigue testing until failure. As it was the case with the cruciform specimens, full fracture was not achieved during the fatigue test, and separation of the specimen in two pieces was managed by using a conventional electromechanics testing machine.

3 RESULTS AND DISCUSSION

3.1 Ultrasonic Cruciform Specimens

After the ultrasonic fatigue tests were completed, the fracture surfaces were observed on microscope, the crack initiation site was identified, the crack initiation angle was measured, and the crack path was analysed. The measured crack initiation angles for three cruciform specimens, under different loading conditions, are shown in Figure 6, and a summary of fatigue life, applied stresses and initiation angle is provided in Table 1. The T-T specimen, Fig. 6 (a), presents a crack initiation angle of 53.9 º, and regarding the C-T specimens, the C-T 1 specimen, Fig. 6 (b), a crack initiation angle of 40.9 º was measured and for the C-T 2 specimen, Fig. 6 (c), the measured crack initiation angle was -23.8 º.

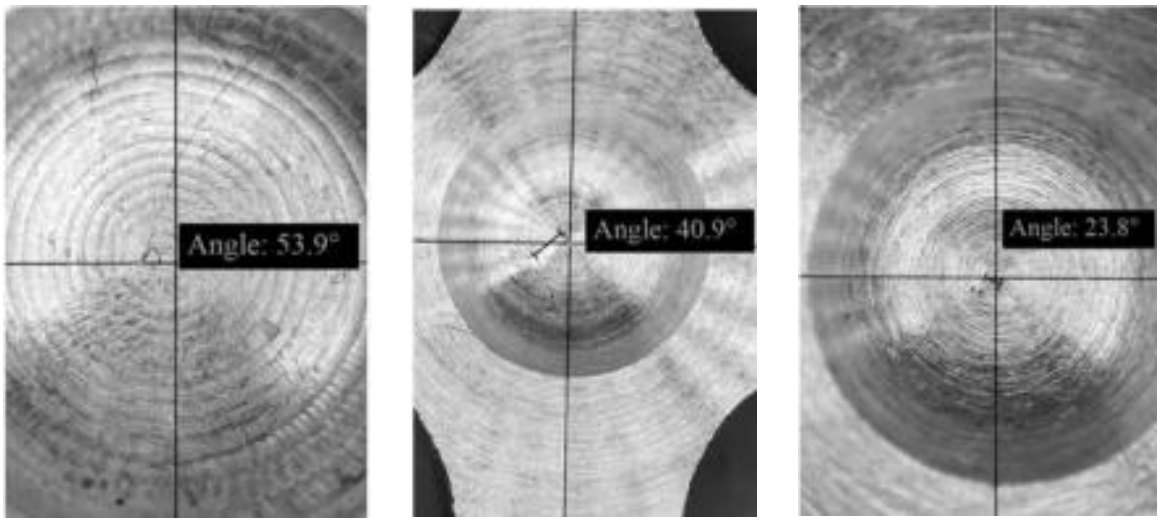

(a) (b) (c)

Figure 6 - Specimen crack initiation angle:(a) T-T; (b) C-T 1; (c) C-T 2.

Table 1 - Fatigue life, stress and crack initiation results

Specimen	Cycles	σ_y [MPa]	σ_x [MPa]	θ [º]
T-T	0.76E6	176.5	174.9	53.9
C-T 1	2.67E6	144.3	137.0	40.9
C-T 2	1.36E7	133.1	124.0	-23.8

A closer examination of the different crack regions of the cruciform specimens provides insight on the evolution of the crack initiation and crack path, respectively. As it can be observed in Figure 7 (a), the T-T specimen presents a single well defined crack propagation path. For the C-T specimens, this is not always the case, with the C-T 1 specimen, Fig. 7 (b), showing in a clear image a crack bifurcation at both ends. D. Infante-García *et al.* [10] have found out that the bifurcation effect occurs when a 45º crack initiates in out-of-phase conditions. In their study, Wolf et al. [11] presented a work with aluminium cruciform specimens where they found out a similar crack behaviour. Moreover, Avateffazeli M. and Haghshenas M., address in their work these topics and they are in consonance.

(a) (b) (c)

Figure 7 - Specimen crack path: (a) T-T; (b) C-T 1; (c) C-T 2.

In addition to the crack initiation and crack path analysis, the cruciform specimen fatigue fracture surfaces were analysed on a SEM. From a raw observation of the fracture surface, it is clear to identify three propagation stages for both kinds of specimens, ie T-T and C-T specimens. Each of these stages shows different characteristics. Figure 8 shows details of the fracture surfaces for specimens T-T and C-T 1.

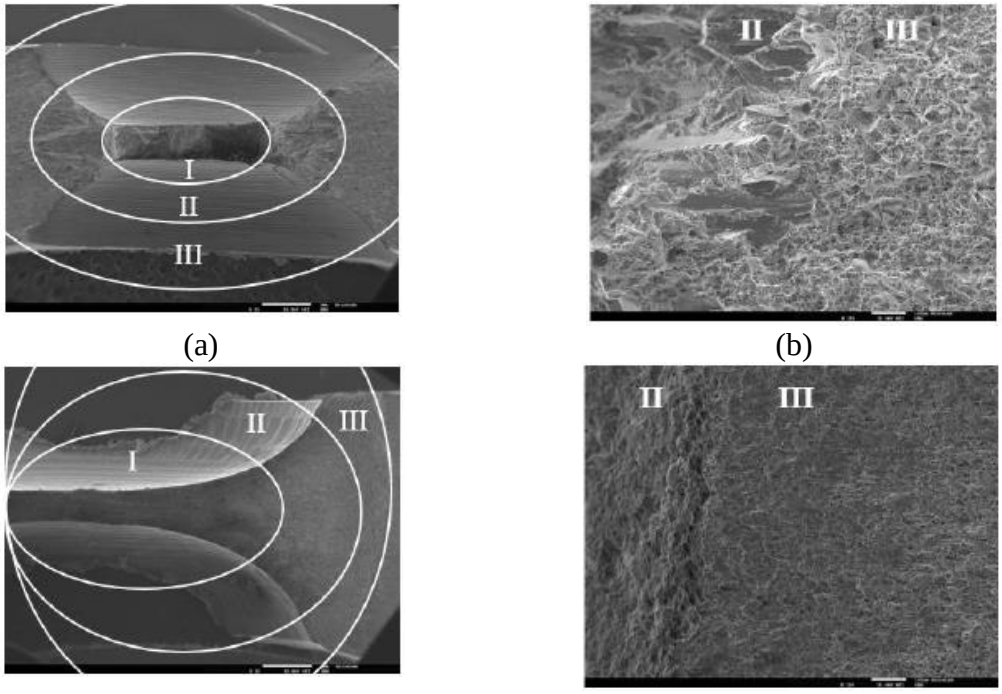

Figure 8 - Cruciform Fracture surface with propagation stages: C-T 1 (a) and (b); T-T (c) and (d).

The propagation stages II and III show different stress combinations and morphologies, when compared to the specimen centre which is predominantly subjected to stage I. These two stages (II and III) also show much higher propagation rates compared with stage I. For the C-T specimen (Fig. 8 (a) and (b)), stage II presents crack mode II while stage III shows signs of normal crack mode I, with tensile dimples which indicate ductile fracture. For the T-T specimen (Fig. 8 (c) and (d)), similar behaviour can be observed between stage II and specimen C-T stage III, however with a different crack propagation rate. Stage III for the T-T specimen presents an elongated dimple type fracture, Fig. 8 (d).

Concerning stage I, which was concentrated in the thinner, central region of the specimen, the crack initiation location can be identified for the T-T specimen, as shown in Figure 9. It is possible to identify multiple mode I crack propagation striations, Fig. 9 A. Also worth a mention are the multiple microcracks that can be observed across the stage I crack surface, Fig. 9 B.

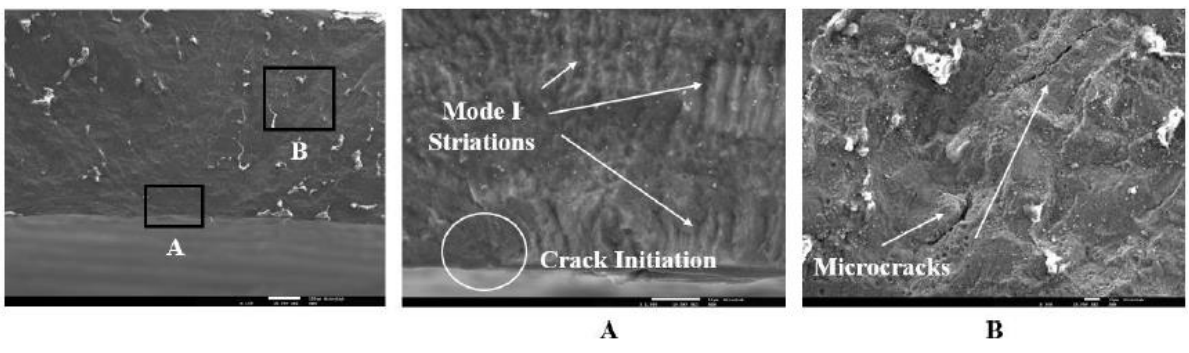

Figure 9 - T-T specimen propagation stage I: (A) Crack initiation and mode I striations; (B) Microcracks.

Contrary to the in-phase specimen (T-T specimen), the C-T specimen does not show a discernible crack initiation location. This suggests that shear is the main fracture mechanism, as stage I fracture surface morphology indicates mixed-mode I and II crack propagation, with shear marks resembling those of high shear stress loaded samples as shown in Figure 10. Figure 10 presents details of fracture surface morphology of a C-T specimen.

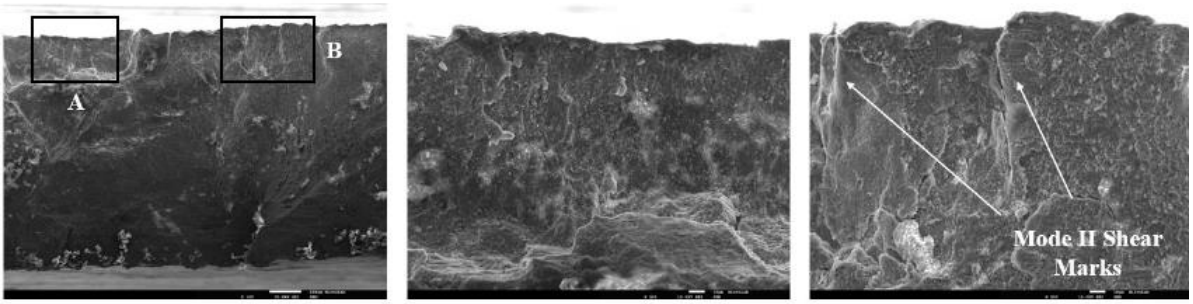

Figure 10 - C-T specimen stage I: (A) Surface crack initiation region; (B) Mode II shear marks.

It is also apparent that mode II is of significant importance for the crack propagation mechanism in stage I. As shown in Figure 11 the flat surfaces are signs of rubbing expected from mode II crack propagation, Fig. 11 (b).

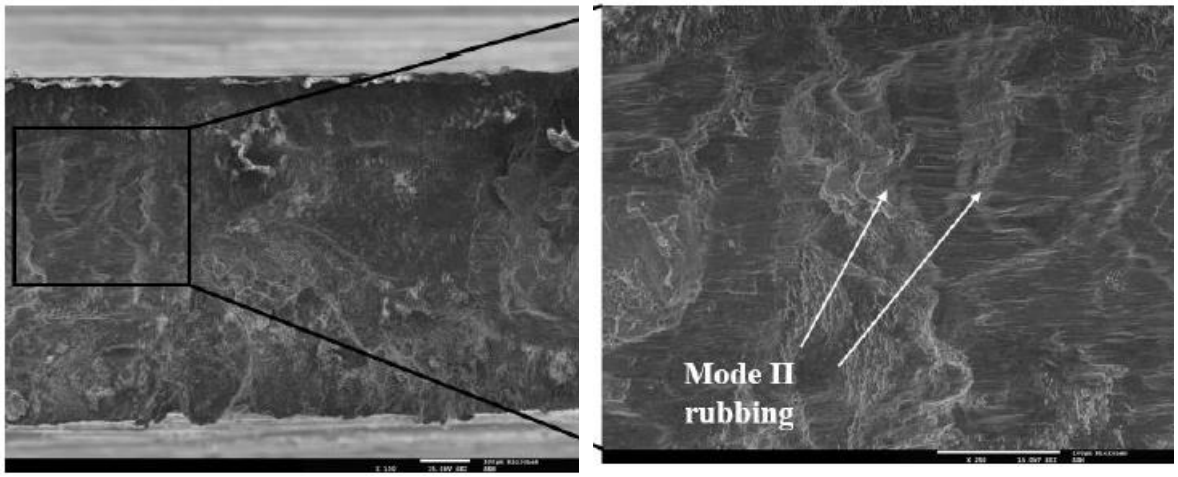

Figure 11 - C-T specimen: (a) fatigue crack surface; (b) mode II shear rubbing marks.

3.2 Ultrasonic Tension-Torsion Specimens

Different shear/axial stress ratio specimens were tested in the experimental campaign. After fatigue testing fracture surfaces were observed and analysed. Tension-torsion specimens present surface crack initiation. The measured crack initiation angle for three different shear/axial stress ratios are presented in Figure 12. A summary of the applied loading (stress components), crack initiation angle and number of cycles to failure is provided in Table 2. The results show for a similar fatigue life a clear correlation between the increase of the stress ratio and the crack initiation angle.

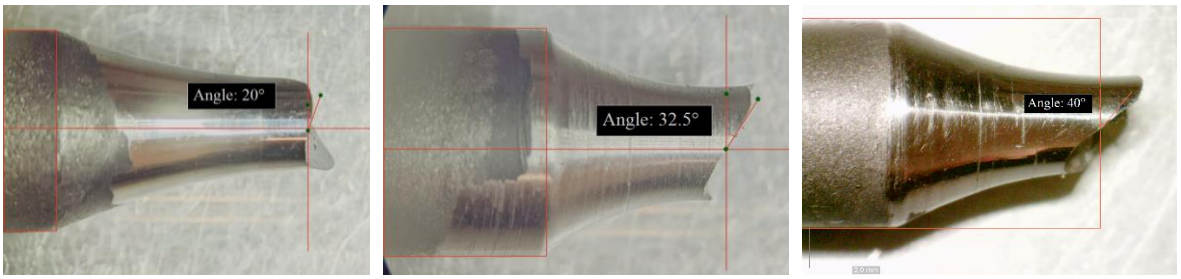

Shear/Axial = 0.38 (a) Shear/Axial = 0.51 (b) Shear/Axial = 1.24 (c)

Figure 12 - Surface crack initiation for different shear/axial ratios (a) 0.38; (b) 0.51; (c) 1.24.

Table 2 - Fatigue testing life, stress and crack initiation angle results

Specimen	Cycles	σ [MPa]	τ [MPa]	τ/σ Ratio	θ [º]
1	9.8E5	484.4	186.3	0.38	20.0
2	3.4E5	373.1	189.9	0.51	32.5
3	1.14E6	266.9	330.8	1.24	40.0

Fatigue fracture surfaces of the aforementioned specimens were analysed at SEM and one image per specimen is shown in Figure 13. An expected mixed-mode I and II crack propagation can be observed for all fracture surfaces in the different stress ratios. A clear trend can be identified as the shear marks are more prevalent as the shear/axial ratio increases, as can be proved from Fig. 13 (a) to Fig. 13 (c). All the images from Fig. 13 are at the same scale.

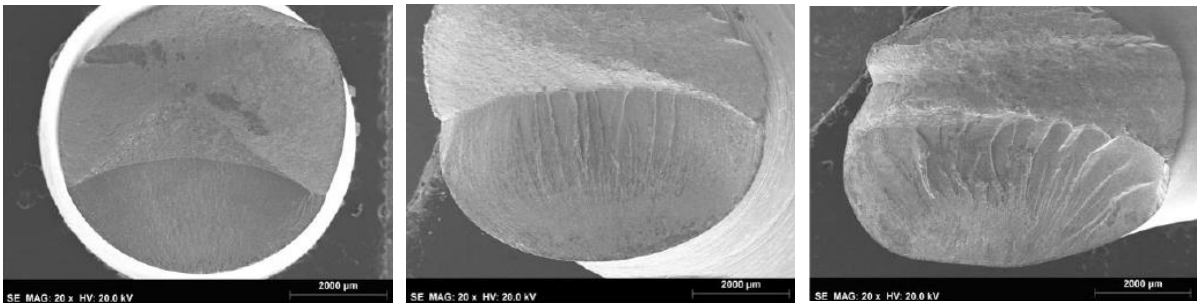

(a) (b) (c)

Figure 13 - Fatigue crack surface for different ratio specimens: (a) 0.38; (b) 0.51; (c) 1.24.

Crack initiation site can be identified by a small dark region for all shear/axial stress ratios. Figure 14 shows an example of the crack initiation site for the 0.51 shear/axial ratio specimen. Analysing in more detail this small dark region, it is possible to observe that the initial stage of crack initiation presents rough local, followed by a smoother surface when crack starts to propagate, gradually transitioning to radial marks more prevalent close to final fracture region.

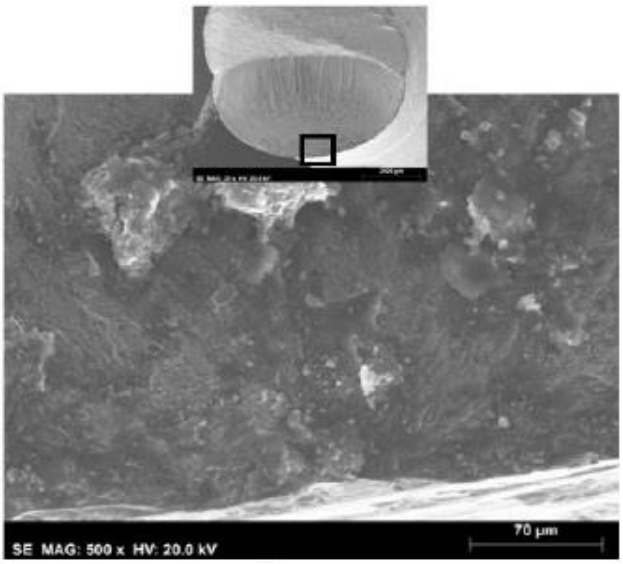

Figure 14 - Fatigue crack initiation site for the 0.51 shear/axial stress ratio.

As can be observed in Figure 15, the increase in size of radial marks suggests a growing influence of shear stress component throughout fatigue crack propagation. As previously mentioned, radial marks and secondary cracks are more prone for higher shear stresses. From the SEM analysis, it is therefore reasonable to state that the fatigue crack propagation is indeed mixed-mode I and II, with increasing influence of mode II.

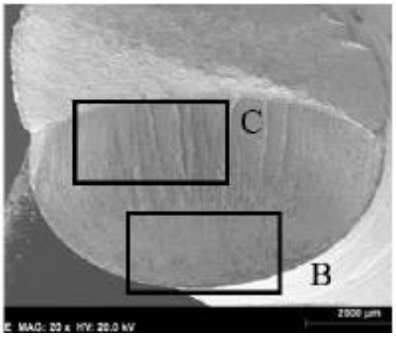

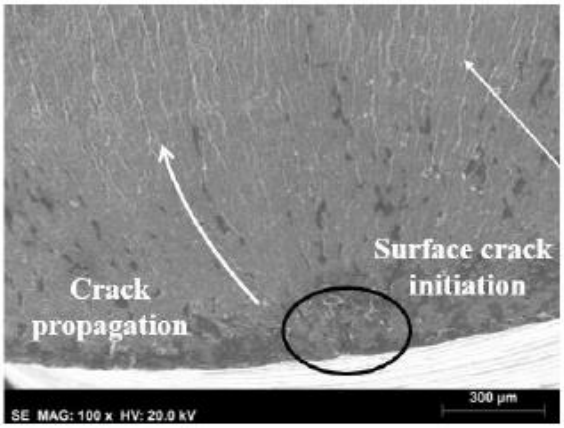

(B)

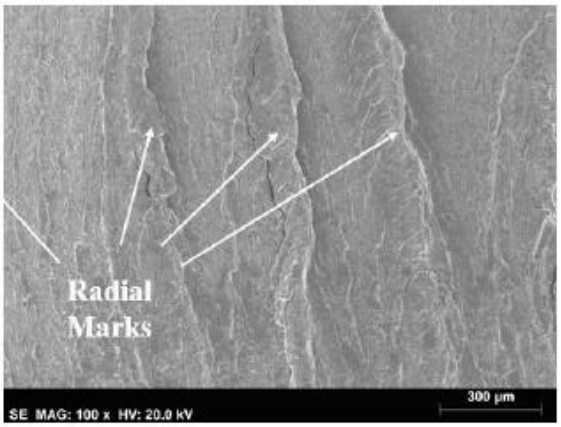

(C)

Figure 15 - Crack propagation details for 0.51 shear/axial stress ratio specimen.

4 CONCLUSIONS

In this work, two different types of ultrasonic multiaxial fatigue testing specimens are successfully tested. Crack initiation angles were measured and crack path trends were observed depending on stress ratios/dimensional changes on specimens. In summary, the main conclusions that can be drawn from this study are as follows:

- Cruciform fatigue testing in ultrasonic fatigue machines was successfully reached;
- Two different cruciform specimens were tested: in-phase Tension-Tension (T-T) and out-of-phase Compression-Tension (C-T);
- Cruciform fatigue fractures were successfully achieved for both kinds of cruciform specimens. Different fatigue fracture surface features were identified and characterized;
- T-T specimens presented mainly mode I crack propagation, while C-T specimens presented mixed-mode I and II crack propagation;
- Tension-Torsion specimens with different shear/axial stress ratios were tested, and the main throat was the region subjected to highest stress amplitude as desired;
- All Tension-Torsion specimens presented surface crack initiation;
- Higher shear/axial stress ratio specimens presented higher crack initiation angles and more predominant torsion fatigue radial marks;
- SEM analysis of Tension-Torsion specimens, provided solid grounds that mode II crack propagation becomes more influent with the increase of the shear/axial stress ratio.

Declaration of Competing Interest

The authors declare that they have no known competing financial interests or personal relationships that could have appeared to influence the work reported in this paper.

Acknowledgements

This work was supported by FCT, through IDMEC, under LAETA, project UIDB/50022/2020. Financial support from Portuguese Fundação para a Ciência e Tecnologia (FCT) is acknowledged through project PTDC/EME-EME/7678/2020.

REFERENCES

[1] C. Bathias, “Piezoelectric fatigue testing machines and devices,” *International Journal of Fatigue*, vol. 28, no. 11, pp. 1438–1445, Nov. 2006, doi: 10.1016/j.ijfatigue.2005.09.020.

[2] P. Costa, M. Vieira, L. Reis, A. Ribeiro, and M. de Freitas, “New specimen and horn design for combined tension and torsion ultrasonic fatigue testing in the very high cycle fatigue regime,” *International Journal of Fatigue*, vol. 103, pp. 248–257, Oct. 2017, doi: 10.1016/j.ijfatigue.2017.05.022.

[3] D. Montalvão and A. Wren, “Redesigning axial-axial (biaxial) cruciform specimens for very high cycle fatigue ultrasonic testing machines,” *Heliyon*, vol. 3, p. 466, 2017, doi: 10.1016/j.heliyon.2017.

[4] A. Nikitin, C. Bathias, and T. Palin-Luc, “A new piezoelectric fatigue testing machine in pure torsion for ultrasonic gigacycle fatigue tests: Application to forged and extruded titanium alloys,” in *Fatigue and Fracture of Engineering Materials and Structures*, Nov. 2015, vol. 38, no. 11, pp. 1294–1304. doi: 10.1111/ffe.12340.

[5] H. Mayer, M. Fitzka, and R. Schuller, “Constant and variable amplitude ultrasonic fatigue of 2024-T351 aluminium alloy at different load ratios,” *Ultrasonics*, vol. 53, no. 8, pp. 1425–1432, Dec. 2013, doi: 10.1016/j.ultras.2013.02.012.

[6] H. Q. Xue, H. Tao, F. Montembault, Q. Y. Wang, and C. Bathias, “Development of a three-point bending fatigue testing methodology at 20 kHz frequency,” *International Journal of Fatigue*, vol. 29, no. 9–11, pp. 2085–2093, Sep. 2007, doi: 10.1016/j.ijfatigue.2007.03.018.

[7] P. R. da Costa, L. Reis, D. Montalvão, and M. Freitas, “A new method for ultrasonic fatigue testing of equibiaxial and pure shear cruciform specimens,” *International Journal of Fatigue*, vol. 152, Nov. 2021, doi: 10.1016/j.ijfatigue.2021.106423.

[8] P. R. da Costa, H. Soares, L. Reis, and M. Freitas, “Ultrasonic fatigue testing under multiaxial loading on a railway steel,” *International Journal of Fatigue*, vol. 136, Jul. 2020, doi: 10.1016/j.ijfatigue.2020.105581.

[9] R. Baptista, R. A. Claudio, L. Reis, I. Guelho, M. Freitas, and J. F. A. Madeira, “Design optimization of cruciform specimens for biaxial fatigue loading,” *Frattura ed Integrita Strutturale*, vol. 30, pp. 118–126, Oct. 2014, doi: 10.3221/IGF-ESIS.30.16.

[10] Infante-García D, Qian G, Migu´ elez H, Giner E. Analysis of the effect of out-of phase biaxial fatigue loads on crack paths in cruciform specimens using XFEM. Int. J. Fatigue 2019;123(January):87–95.

[11] Wolf CH, Henkel S, Burgold A, Qiu Y, Kuna M, Biermann H. Investigation of fatigue crack growth under in-phase loading as well as phase-shifted loading using cruciform specimens. Int. J. Fatigue 2019;124(February):595–617.

[12] Avateffazeli M, Haghshenas M. Ultrasonic fatigue of laser beam powder bed fused metals: A state-of-the-art review, Engineering Failure Analysis, Volume 134, 2022.